

OVERVIEW OF THE R&D PROGRAM FOR THE SPALLATION NEUTRON SOURCE TARGET

J. R. Haines, D. K. Felde, B. W. Riemer, C. C. Tsai, and M. W. Wendel
Oak Ridge National Laboratory
701 Scarboro Road
Oak Ridge, TN 37922, USA
Phone: (865) 574-0966
e-mail: hainesjr@ornl.gov

Keywords: target, neutron, source, mercury, spallation.

ABSTRACT

The R&D program for the Spallation Neutron Source (SNS) mercury target addresses issues associated with the quasi-static power handling and the effects of pressure waves created by the pulsed energy deposition. Three flow loops have provided the data necessary to confirm that mercury can transport the deposited proton beam power away from the target while also serving to adequately cool the stainless steel target vessel. Pressure pulse effects studies have considered (1) the disturbance of the flow, (2) the strains induced in the mercury container, and (3) the erosion caused by cavitation bubble collapse. Progress on these items including recent results of accelerator target tests and efforts to understand the erosion scaling is discussed.

1. INTRODUCTION

The mercury target for the Spallation Neutron Source (SNS) must be designed to sustain a time-averaged proton beam power of 2 MW, which is deposited in nearly instantaneous ($< 1 \mu\text{s}$) pulses at a 60 Hz repetition rate (Gabriel, 2002). A mercury target development program, aimed at defining a system that can remove the power deposited in the target without excessive temperatures or stresses, was established

several years ago (Haines, 1996). This program, which continued to evolve as experimental results became available, focused on studying the thermal hydraulic, thermal shock (effects of intense power deposition from pulsed-beam), and materials irradiation and compatibility phenomenon. To conduct these studies, we constructed and operated several flow loops, performed tests at accelerator facilities, and used the experimental results to benchmark computer models. This paper addresses only the thermal hydraulic and thermal shock aspects of the SNS Target R&D effort, but a brief summary of the target design is also provided.

Mercury, rather than a water-cooled solid heavy metal, was selected as the target material for SNS primarily because of its potential for increased power handling capability and greatly reduced waste stream. The design concept for the liquid mercury target, which is shown in Fig. 1, has a width of about 400 mm, height of about 100 mm, and an effective length for neutron production of 700 mm.

The mercury is contained within a structure made from 316-type stainless steel. Mercury enters from the back side (side opposite the proton beam window) of the target, flows along the two side walls to the front surface (proton beam window), and returns through a 206 mm x 80 mm rectangular passage in the middle of

the target. The target window, i.e., the portion of the target structure in the direct path of the proton beam, is cooled by mercury which flows through the passage formed between two walls of a duplex structure. In this way, the window cooling and transport of heat deposited in the bulk mercury are achieved with separate flow streams. This approach is judged to be more reliable and efficient (minimal pressure drop and pumping power) than using the bulk mercury to cool the window. Also, the duplex structure used for the window has significant structural advantages that help to sustain other loads. Besides serving as flow guides, the baffle plates used to separate the inlet and outlet flow streams are important for maintaining the structural stability of the target.

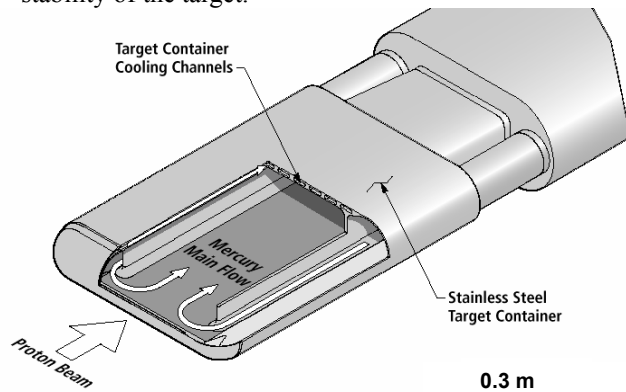


Fig. 1 SNS mercury target design showing cooling channels (cooling jacket) and flow baffles that are used to separate the main (bulk) flow inlet and outlet streams.

The mercury target R&D program addresses both the overall quasi-static power handling and the effects of pressure waves created by the pulsed energy deposition resulting from the interaction of the mercury with the proton beam. The portion of the R&D work associated with the transport of the time-averaged, i.e. quasi-steady state, power deposited by the beam is referred to as the Thermal Hydraulics R&D. Three test loops were constructed to supply the data necessary to confirm that mercury can transport the deposited proton beam power away from the target while also serving to adequately cool the stainless steel target vessel. The measurements also provide benchmark data for developing computational fluid dynamics (CFD) models that are being used as engineering design and analysis tools.

The portion of the R&D program aimed at developing a target vessel and flow system that can withstand the pressure pulses resulting from the isochoric heating conditions in the target is referred to as the Thermal Shock R&D program. This portion of the program includes: (1) fundamental pressure pulse and cavitation experiments in off-line laboratory tests, and (2) pulsed-proton beam tests of mercury targets at accelerator facilities.

Details of the thermal hydraulic and thermal shock work conducted to support the SNS target development program are described below.

2. THERMAL HYDRAULIC R&D

A series of experimental and computational investigations aimed at characterizing the quasi-static power handling behavior of the proposed design for the SNS target have been completed. To assure reliable and safe operation, several specific areas were addressed. These include the wettability of liquid mercury on stainless steel surfaces with corresponding effects on heat transfer and frictional pressure drops, and the fluid flow characteristics of the bulk flow in the target and cooling jacket regions where the proton beam deposits its energy.

Fluid flow characteristics of the target are simulated using computational fluid dynamics (CFD) models. The CFX4 general-purpose CFD code was utilized with the RNG k-epsilon turbulence model option and a turbulent Prandtl number of 3.1 assumed for the liquid mercury flow. Validating and benchmarking these models under the hydraulic conditions of the actual target is necessary to develop confidence limits for application to design and analysis of thermal hydraulic performance. The three experimental test facilities used to evaluate the thermal hydraulic issues described above and benchmark the CFD models include the Mercury Thermal Hydraulic Loop (MTHL), the Water Thermal Hydraulic Loop (WTHL), and the Target Test Facility (TTF). These facilities and accompanying CFD efforts are discussed below.

Mercury Thermal-Hydraulic Loop (MTHL)

An experimental test facility was constructed to evaluate heat transfer and wetting characteristics in flowing liquid mercury channels with geometric shapes and flow velocities similar to those planned for the SNS target (~ 3.5 m/s). Loop components were selected to provide SNS heat flux levels and temperatures and flow rates corresponding to those in the passages of the target cooling jacket.

The flow loop components are constructed primarily of 316 stainless steel. A variable speed, electromagnetic pump, fabricated by the Institute of Physics at the University of Latvia, provides the driving force for circulating the mercury through the test section and heat exchanger. A list of nominal operational parameters for the MTHL facility is provided in Table 1.

Table 1. MTHL Operational Parameters

Parameter	Value
Loop Hg Volume	~ 20 L
Material	316 SS
Operating pressure	0.1 – 1.3 MPa
Maximum Temperature	250 °C
Maximum flow rate	6 kg/s
Pump head	0.25 MPa
Tubing inner diameter	32 mm
Power supplied to pump	20 kW

Several test sections have been used to provide the required data over a wide range of inlet temperatures (80 to 220 °C), pressures (from 0.1 to 0.4 MPa) and velocities (from 1 to 4 m/s). As shown in Fig. 2, the measured non-dimensional heat transfer data agrees well with computational fluid dynamics calculations (Wendel, 2000) (Crye, 2001). All tests have achieved excellent heat transfer, and no evidence of the conditions previously attributed to “non-wetting” has been observed.

Water Thermal Hydraulic Loop

The Water Thermal Hydraulic Loop (WTHL) was used to evaluate flow characteristics in the target bulk flow, especially in the recirculation and stagnation regions. A full scale mockup of the bulk flow passages within the SNS target assembly was fabricated using stereo lithography in a molding process to accurately model the interior design details. The front 0.59 m of the target is constructed of transparent plastic to provide access for flow visualization studies and velocity distribution measurements using a Laser Doppler Velocimeter (LDV) and an Ultrasonic Velocity Profiler (UVP). A photograph of the test section installed in the loop is shown in Fig. 3.

Test objectives for the WTHL include benchmarking CFD models, examination of the effect of design changes on the target fluid performance (e.g. baffle location), and evaluation of diagnostic methods which may be applicable to mercury tests in the Target Test Facility (TTF), which is described later. Measurements made in the WTHL include flow rate for

each inlet, pressure drop across the test section, pressure measurements at selected locations in the transparent front section, detailed localized velocities and velocity vectors in the transparent section using a 2-D LDV system, and flow visualization studies using injected dyes and gas bubbles.

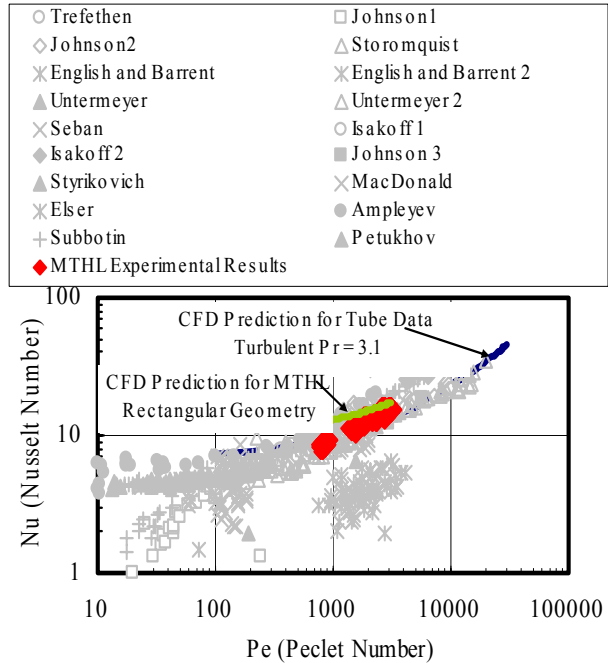


Fig. 2 Measured heat transfer coefficient for coolant channels simulating the target coolant passages (data taken from JSME Data Book: Heat transfer 4th Edition).

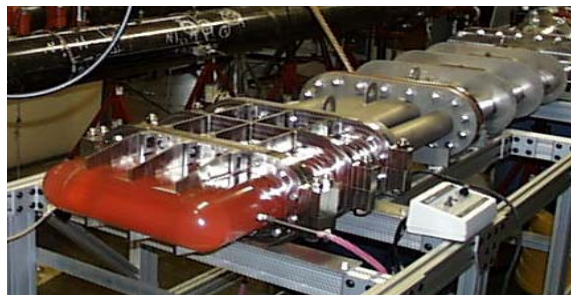


Fig. 3 Transparent test section (full-scale model of the target bulk flow region) in the Water Thermal Hydraulic Loop.

The nominal volume flow rate of water in the WTHL tests is the same as the volume flow rate of mercury in the actual target. For these conditions, the Reynolds number in the water flow experiment is 1.4 x

10^5 , which is about one order of magnitude lower than the value for the nominal mercury flow. With this difference in Reynolds number, the time-averaged flow velocity and turbulence intensity are expected to be well matched to the SNS target; however, the WTHL cannot be expected to accurately simulate the dynamic behavior of the flowing mercury system, such as turbulent pressure fluctuations and flow stability, which are density-driven effects.

The time-averaged velocity parallel to the proton beam (predominant flow direction) measured with the LDV system is shown in Fig. 4 at various locations along the horizontal mid-plane of the target. CFD predictions are also shown in this figure for comparison. The CFD results show overall good agreement with average velocity and turbulent intensity measurements, with a slight over prediction of the size of the flow reversal region near the front of the baffles (Pointer, 2000) (Wendel, 2001).

Target Test Facility

The Target Test Facility (TTF) provides a full-scale test bed for performing thermal-hydraulic tests using mercury. A photograph of the facility is shown in Fig. 5. The primary purpose of the thermal-hydraulic tests conducted in this facility was to provide confirmation that the full scale target meets its design requirements with mercury as the fluid. It is not practical to impose prototypic heat loads at this scale, so the tests and measurements focused primarily on the hydraulic aspects of the target. In addition, CFD models have been benchmarked with UVP measurements.

The TTF mercury process system contains components representative of the SNS Target Cell equipment. It is constructed primarily of stainless steel with piping ranging in size from 50 mm to 200 mm in diameter. A centrifugal pump located in a sump tank provides the driving force for mercury flow and is powered by a 56 kW motor with variable speed control ranging from 60 to 600 rpm. The nominal flow to the target is 24 L/s, consisting of 11.2 L/s in each of the two bulk feed lines and a simulated-cooling jacket flow of 1.6 L/s. Flow to the target is adjusted by manual throttle valves located in each bulk feed line and in the cooling jacket feed line. Venturi flow tubes are used to measure flow in each of the target feed and return lines. The process also includes a mock heat exchanger in the return line, a mercury storage tank and a centrifugal pump for transferring mercury from the storage tank to the loop. A functional heat exchanger was installed in the window feed line for removing frictional heat.

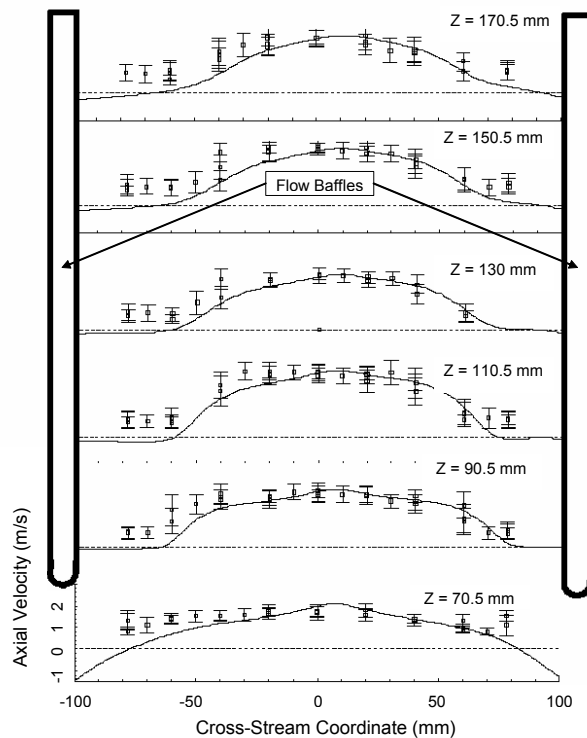


Fig. 4 Comparison of measurements (symbols) with CFD predictions (lines) of the axial velocity in the return channel of the bulk flow region at the horizontal mid-plane (Z = distance from the front of the target).

The TTF loop contains 1.4 m³ of elemental mercury weighing approximately 19,000 kg. The presence of mercury in the system requires an enclosure to provide secondary containment. The enclosure was constructed as two separate cells with a common wall. One room houses the process equipment, the other houses the target and interconnecting piping between the cells. Wall-to-wall stainless steel floor pans were installed in each enclosure room to prevent any liquid mercury from escaping from the enclosure.

Initial tests were conducted to verify hydraulic performance of the pump and piping system. This testing did not utilize a prototypic target design, but rather a flow jumper in place of the target. Testing in this configuration was of limited scope and used primarily to address general target flow supply questions. This included measurement of flow rate, flow splits, and pressures for confirmation of overall friction factors and pressure drops within the piping system. In

addition, performance of the pump with mercury was compared with manufacturer supplied pump curves.

A second testing phase used a prototypic test section to examine the bulk flow within the target at full scale. A photograph of the target prototype is shown in Fig. 6. Velocity profiles in the bulk flow channel were measured using an Ultrasonic Velocity Profilometer (UVP). These measurements were performed to characterize the flow distributions, including recirculation and stagnation zones for comparison with CFD predictions. Typical results for the velocity near the center of the target are displayed in Fig. 7 for 50% nominal flow conditions. Except in regions near the stainless steel wall/mercury interface (0-0.25 m in Fig. 7), where the measurements are unreliable due to the erratic behavior of the sensor system, the measurements are reasonably matched by CFD predictions (Felde, 2001) (Wendel, 2001).



Fig. 5 Photograph of the TTF, which is a full-scale model of the SNS mercury flow loop.

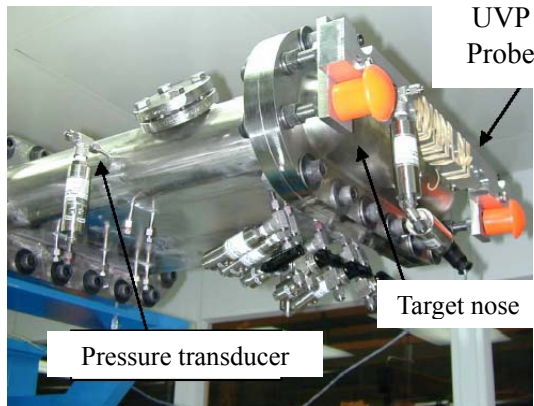


Fig. 6 Photograph of the target prototype used in the second TTF testing phase to measure velocity profiles with the UVP device.

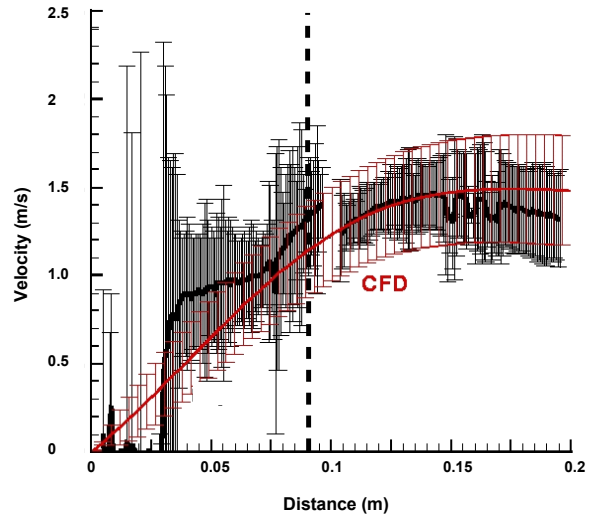


Fig. 7 Measured and predicted axial velocity profiles near the centerline of the target (measured data shown in black and CFD predictions shown in red).

3. THERMAL-SHOCK R&D

One of the most challenging issues associated with applying liquid metals as targets for pulsed proton beams is withstanding the effects of the intense heating of the liquid metal from individual pulses of protons. Although the resulting temperature rise for a single pulse is relatively small (~ 10 K in the peak location), the rate of temperature rise is enormous ($\sim 10^7$ K/s) during the very brief event (~ 0.7 μ s). This heating occurs essentially instantaneously compared to acoustic wave time scales; therefore, the mercury undergoes a large pressure increase. The resulting compression of the mercury leads to the production of large amplitude pressure waves in the mercury that interact with the walls of the mercury target and the bulk flow field.

There are three primary concerns associated with this pressure increase. First, the mercury container must be able to withstand the strains caused by the pressure pulse. Second, the flow that is required to transport the beam power must not be unduly impeded. Third, the erosion caused by cavitation bubble collapse must be slow enough to yield a reasonable target vessel lifetime. Thermal shock R&D efforts on each of these items are described below.

Vessel Strains

A series of tests were conducted at Los Alamos National Laboratory's Weapons Neutron Research (WNR) facility to study the strain response for simple

target container shapes. The WNR beam parameters are summarized in Table 2. Although total energy per pulse deposited in the mercury in these tests (~2.2 kJ) is substantially lower than in the SNS target (~20 kJ), by tailoring the beam size, the maximum energy density in test targets can be made comparable to that in SNS (12 MJ/m³). Using test targets that were roughly 1/3-scale of the SNS target, the proportion of the beam cross-sectional area to the target cross-sectional area is also comparable. The target geometry used in most of these tests is shown in Fig. 8, and is referred to as a “Large Effects” (LE) type because the pressure pulse will produce a large strain in the thin diaphragms (~1 mm thickness) used as end plates. The LE target has a simple cylindrical shape with a 100 mm diameter and 286 mm overall length.

Fiber-optic based sensors based on the Fabry-Perot interferometer principle were successfully used to gather data under prototypical beam intensities (Cates, 2001). Typical strain responses for the end plate of a simple cylindrically shaped LE target are shown in Fig. 9 for four consecutive pulses. This particular strain sensor was positioned about 25 mm from the center of the rear diaphragm and oriented radially. The radial strain response exhibits excellent pulse-to-pulse repeatability.

These data show a frequency response that is much lower than initially predicted, but the magnitude of the strain range is close to the predicted values for most cases (Riemer, 1999). It is speculated that the reason for the lower than expected frequency response is the presence of cavitation bubbles in the mercury, which could significantly reduce the sound speed in the bubble-liquid mixture.

Recent predictions, using conventional finite element models with modified equations of state for mercury that account for cavitation, have improved the match between measurements and predictions to the point where the numerical model will be used to evaluate the actual SNS target under a series of normal and off-normal conditions. Strain ranges will be used along with fatigue design data gathered under the SNS materials qualification program to size structures and verify the adequacy of the target vessel design.

Effect of Pressure Pulse on the Mercury Flow

Although no in-beam tests have been conducted with flowing mercury, a CFD calculation was made for a simplified and conservative boundary condition at the mercury wall interface. The container walls were assumed to be perfectly rigid, thus leading to complete reflection of the pressure. Results of these calculations show that although the flow along the inlet channel are

greatly reduced in the time period immediately following a beam pulse, the flow completely recovers in less than a millisecond. Since there are 16.7 ms between successive pulses in SNS, the flow is well established before the next pulse arrives. Simple energy balance arguments also show that the mechanical energy input to the system from the pressure rise is much less than the pumping power in the flow system.

Table 2. Beam parameters for WNR tests

Parameter	WNR	SNS (@ 2 MW)
Proton Energy (GeV)	0.8	1.0
Protons/pulse (Tera-protons)	28	200
Energy deposited in mercury target (kJ)	2.2	20
Maximum energy deposition density (MJ/m ³)	4-18	12

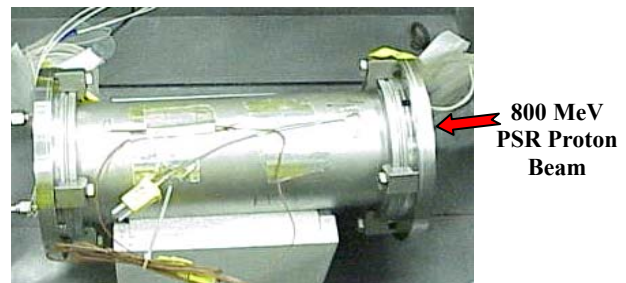


Fig. 8 “Large Effects” target used for mercury target pitting tests at the WNR facility.

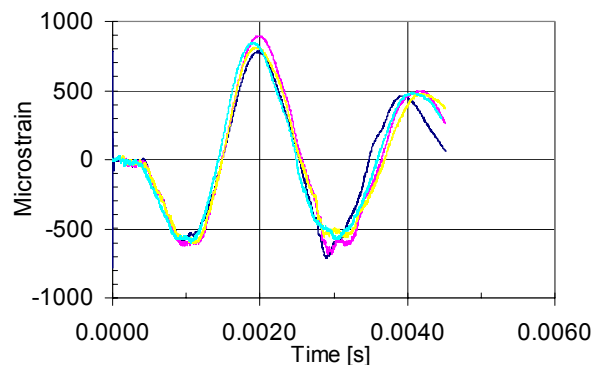


Fig. 9 Typical strain response for an LE target tested at the WNR facility in July 2000.

Cavitation Pitting Erosion

A team of researchers at the Japan Atomic Energy Research Institute (JAERI) first observed pitting of stainless steel surfaces that were in contact with mercury subjected to large mechanically induced pressure pulses of the same magnitude as those expected at full power (2 MW) pulses in SNS (Kikuchi, 2002). The question then became; do the surfaces of liquid mercury target containers with comparable beam-induced pressure pulses also pit? Post-irradiation examinations of targets previously used in pulsed proton beam tests were unable to resolve this question because no pre-test inspections had been performed and the roughness of the surfaces was too great to distinguish between beam-induced pits and other imperfections in the surface of the materials.

Earlier tests within the SNS target development program had shown that mercury, with the level of impurities and dissolved gasses expected in the SNS process loop, will cavitate when the tensile pressure reaches only a few atmospheres (Taleyarkhan, 2000) (Moraga, 1999). These types of conditions will exist in the target immediately following a proton pulse, due to the reflection of the initial compression wave as a rarefaction wave from the interface between the walls of its container and the surrounding environment. It is well known that cavitation bubble collapse can eventually cause severe damage to surfaces.

Tests conducted during 2001 were designed to examine whether the pressure pulse phenomenon causes pitting damage to the stainless steel container for the mercury. Cylindrically shaped targets of the type previously used for strain measurements (LE type) (see Fig. 8) were used for the initial cavitation damage tests.

All four of the diaphragm flanges tested in July 2001 were fabricated from 316 type stainless steel in the annealed condition. Three of them were used directly, whereas the fourth was first treated with a surface hardening technique. Large pits, visible to the naked eye, were found near the center of all diaphragms. Small, randomly distributed pits were found on the bare diaphragms, while no pits of this type were found on the treated diaphragm (Haines, 2001).

Based on the July 2001 test results, it was concluded that some means to mitigate this pitting damage is required to ensure that the mercury target can achieve an acceptable lifetime in the SNS facility. With this in mind, the December 2001 tests were dedicated to further examining the pitting phenomenon and looking at an array of possible solutions, or at least reductions, to the pitting problem.

Six mercury targets were tested in the December 2001 campaign. Four of the mercury targets used

different shapes or different diaphragm materials and were exposed to 200 beam pulses. Most notably, a target with a rectangular cross section was used in an attempt to eliminate the postulated radial focusing of the pressure wave. Also, diaphragms with increased thickness, intended to reduce the large stresses, were tested. Two mercury targets were tested with only 20 pulses to determine whether future tests might be possible at this reduced fluence level.

Two results from these tests are especially noteworthy. First, a highly cavitation damage resistant cobalt alloy (Stellite 6B) was severely pitted. Second, the only surface that survived the tests with no pitting was a thick-walled flange made from 20% cold-worked 316 SS that had a surface hardening treatment called Kolsterizing. More detailed discussions of the results of these tests are given by Riemer (2002) and Hunn (2002).

With cavitation erosion concerns in mind, a set of criteria for deciding whether or not to maintain mercury as the target material were established in April 2002. The criteria were that (1) WNR tests for a target geometry and material combination must show pitting damage that can be scaled from 100-200 test pulses to at least 14 days of operation in SNS at 1 MW proton beam power, (2) the high cycle scaling behavior of "high pressure pulse" pitting damage must be demonstrated up to at least one million cycles for materials similar to those successfully tested at WNR, and (3) these results must be available for making a final decision by October 15, 2002.

Twenty-one targets were tested in the June 2003 WNR tests, including variations in target material, geometry, power level, use of gas injection to mitigate the damage, and number of beam pulses (one test ran for 1,000 pulses, which represents an order of magnitude increase over the nominal 100 pulses). Most of the targets utilized a rectangular geometry as shown in Fig. 10. Highly polished front and rear end-plates were used as the primary test specimens to measure the degree of pitting damage. A highly polished plate was also inserted near the bottom of most targets to simulate the small slots used in the SNS target for the target container cooling passage.

Pre-test SEM examinations were performed on all of the polished plates. A 5 x 5 array of micro-indentation marks were applied on each plate to serve as fiducial marks for pre- and post-test images. These marks were centered on the plates and spaced on an orthogonal grid with a spacing of 5 mm. Images with magnifications of 100x and 400x were recorded at each mark.

The WNR tests were successfully conducted and the irradiated targets were returned to ORNL for

mercury decontamination followed by post-test SEM examinations. Pitting damage was determined using image processing software (Price, 2003). The pitting was characterized primarily using two parameters. The first was simply the fraction of area that was damaged. Data are quoted for the worst SEM image found on a specific plate. The second is the mean depth of erosion (MDE) for the SEM image with the worst damage. The MDE was calculated by determining the area of each individual pit on an SEM image, calculating an equivalent radius, and assuming that the pit has a conical shape with a depth equal to its radius. Based on a limited amount of profilometry measurements, this assumption likely overestimates the pit depth by as much as an order of magnitude.

The reference test case was the rectangular target with 20% cold-worked 316 SS plates subjected to a beam intensity that gave a volumetric energy deposition equivalent to that for SNS operating at 2.5 MW with a 60 Hz repetition rate. Pre- and post-test SEM images for the reference case at the location that exhibited the most severe cavitation pitting damage are shown in Fig. 11. The corresponding pitting statistics computed for this case are also included in the figure. In this worst location, almost 5% of the surface is covered with pits and the MDE is 132 nm.

Results for six of the targets are summarized in Table 4. These data were taken from the front plate of each rectangular cross-section target. The equivalent power level, as scaled from the peak energy density within the target, is shown in this table to facilitate comparisons.

The strong dependence on energy density (power level) is quite remarkable. Reducing the equivalent power level from 2.5 MW to 1.1 MW reduces the mean depth of erosion by more than an order of magnitude. Data for the lowest power level (0.4 MW equivalent) are unreliable since the number of pits in the worst SEM frame is too small to be statistically significant.

Increasing the number of beam pulses by an order of magnitude has little effect on the damage, thus indicating a weak dependence on this parameter, consistent with the classical cavitation data in the so-called incubation regime.

Injecting a layer of gas along the front plate also reduced the erosion by more than an order of magnitude. Based on pre-test videos, the gas layer was imperfect, covering the beam interaction region of the plate about 80 % of the time. Improvements in this concept could lead to further reductions in the cavitation damage. Additional tests, not shown in Table 4, with tall, thin targets showed that injection of bubbles reduced the erosion by about a factor of four compared to an

equivalent target without bubbles. The bubble injection concept can likely be greatly improved as the first operation of the bubble injection system in this configuration occurred moments before the in-beam test.

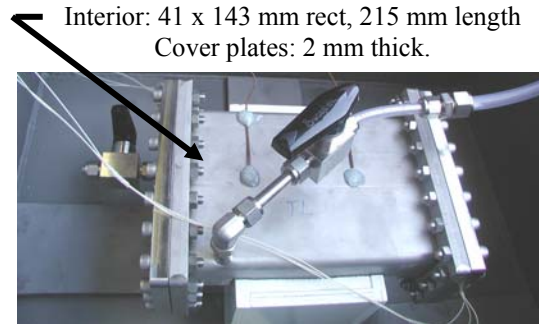
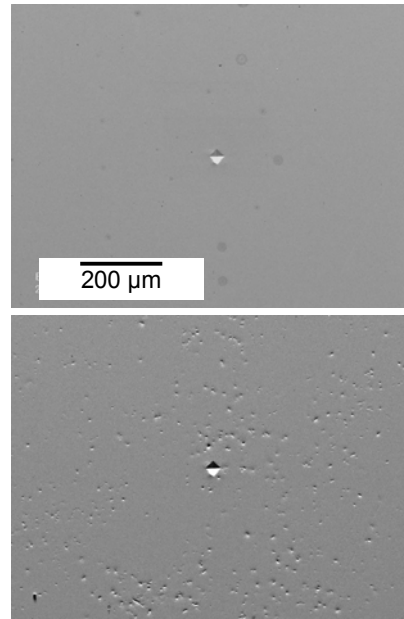


Fig. 10 One of the rectangular targets used in the pitting tests conducted at the WNR facility in June 2002.



Equivalent SNS Power Level = 2.5 MW

Summary for Worst Image	
Image # 25665	
Fraction of Area with Pits	0.046
Average Pit Area (μm^2)	30
Diam of Ave Area Pit (μm)	6.2
Max Area of Pit (μm^2)	1600
Diam of Max Pit (μm)	45.0
Mean Erosion Depth (nm)	132.0

Fig. 11 SEM images and pitting statistics for the reference case from July 2002 WNR tests.

The results for the target plate treated with the Kolsterising process showed essentially no pitting damage for the 100-pulse test. This process involves diffusion of carbon in the near surface material thereby insuring that the treatment is graded, i.e. no sudden changes in properties such as those typically encountered with hard coatings. Characterization of the treated layer has shown that although it is about five times harder than annealed 316 SS it maintains excellent toughness. The primary uncertainty in utilizing this treatment is whether or not it maintains its properties after significant irradiation.

Four off-line test apparatuses were used to help extrapolate this in-beam data from the limited number of beam pulses to the lifetime goal of 7×10^7 . The SNS team built a simple drop test device based on the principles of the Split-Hopkinson Pressure Apparatus used earlier by the JAERI team (Kikuchi, 2002) to discover the pitting problem. The SNS team also continued to use an ultrasonic horn operating at 20 kHz (Kass, 1998) (Pawel, 2002). A collaborative effort was also established with Robin Cleveland of Boston University to use their lithotripter (kidney stone blaster) to create cavitation pits on small specimens. The JAERI team, led by Masatoshi Futakawa, built a magnetically driven impact test device called the Magnet Impact Test Machine (MIMTM) (Futakawa, 2003).

All of these devices succeeded in creating pitting damage similar to that observed with the beam tests, although in some cases it took many more or many fewer pulses to reach an equivalent level of damage. The apparatus that best matched beam damage on a pulse by pulse basis was JAERI's MIMTM device.

A summary of the in-beam and off-line cavitation damage test results is shown in Fig. 12. It should be noted that these data exhibit the usual cavitation damage behavior. That is, early in the process, called the incubation regime, very little erosion occurs, while the erosion eventually reaches the "steady state" regime, where the erosion rate is proportional to N^α , with N being the number of cycles and α being a constant that apparently depends on the fluid. The duration of the incubation period depends upon the test conditions. It appears that the damage from the WNR 1.1 MW equivalent case is less severe than that for the MIMTM device. Therefore, it is concluded that the MDE for the 1 MW SNS target would be less than 50 μm after two weeks of operation. Although the failure mechanism is not understood, this amount of erosion is judged to be acceptably small.

Table 4. Summary of pitting damage on the front plate of rectangular shaped targets tested at the WNR facility.

Target	Equivalent SNS Power Level (MW)	Fraction of Area with Pits (%)	Mean Depth of Erosion (nm)
High Power	2.5	4.6	132
Medium Power	1.1	0.3	12
Low Power	0.4	0.2	4
1,000 Pulse	2.9	3.6	101
Bubble Layer	2.7	0.3	8
Kolsterized	3.1	0.03	0.1

All targets, except KILO, exposed to 100 WNR beam pulses
All plates except the Nitronic 60 plate were constructed from 316 type stainless steel

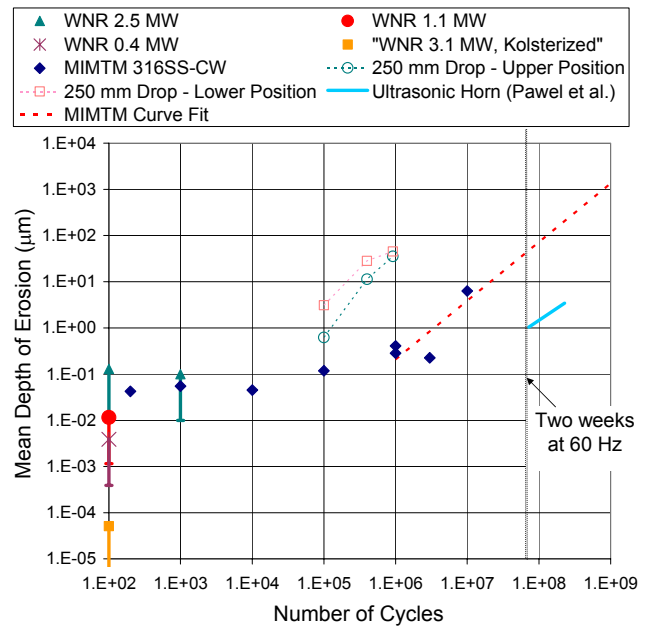


Fig. 12 Summary of pitting damage tests.

4. CONCLUDING REMARKS

The SNS mercury target development program is nearly completed. Three flow loops were constructed to address the thermal-hydraulics issues. Using these facilities and CFD models, the local heat transfer and stability characteristics of the entire system were demonstrated. By operating these facilities, the SNS team gained significant operational experience with a prototypical pump, heat exchanger, seals, valves, etc.

Significant progress has also been made on the thermal shock issues. Recent efforts aimed at quantifying the pitting damage from in-beam tests have been successful. Pitting damage appears to be especially sensitive to beam intensity, surface treatment (Kolsterizing), and gas injection. Off-line pitting simulation tests have provided understanding of how damage scales with cycles. Using the results of the off-line tests to scale the results from the in-beam tests, it is concluded that the mercury target decision criteria of achieving at least a two-week lifetime at an operating level of 1 MW has been satisfied. However, significant uncertainties and associated risks remain. Further R&D and target design efforts are needed to verify these conclusions and extend the target to higher operating powers and longer lifetimes.

ACKNOWLEDGEMENTS

The authors wish to thank the entire SNS Target R&D team for their contributions to this large effort. Obtaining the more than 6,000 SEM pre- and post-test images was a formidable task that was only made possible by the efforts of a large group of SNS engineers and scientists who volunteered over a three month period to perform this work on nights and weekends. Special thanks also to our collaborators at JAERI, especially Masatoshi Futakawa, who developed the MIMTM device and along with his team conducted many tests that were critically important to our decision making process, at Forschungszentrum Jülich, especially Helmut Soltner, for conducting the bubble injection target tests, and at Los Alamos National Laboratory, especially Steve Wender, Bruce Takala, Gregg Chaparro, and Valentina Tcharnotskaia, for their help in conducting the mercury target tests at WNR. This work has benefited from the use of the Los Alamos Neutron Science Center at the Los Alamos National Laboratory. This facility is funded by the US Department of Energy under Contract W-7405-ENG-36.

REFERENCES

Cates, M. R., et al., 2001, SNS Project Report Number SNS-101050200-TR0009.

Crye, J. M., et al., 2001, ASME Journal of Heat Transfer.

Felde, D. K., et al., 2001, SNS Project Target Systems Report TSR-216.

Futakawa, M., 2003, 11th Intl. Conf. on Nuclear Eng., ICONE11-36175.

Gabriel, T. A., Haines, J. R., and McManamy, T. J., 2002, Proc. 5th Int. Workshop on Spallation Mats. Tech.

Haines, J.R., et al., 1996, Int. Workshop on Technology and Thermal Hydraulics of Heavy Liquid Metals.

Haines, J. R., et al., 2001, LANSCE Activity Report 2001, LA-13943-PR, p. 74.

Hunn, J.D., Riemer, B.W., and Tsai, C.C., 2002, Proc. 5th Intl. Workshop on Spallation Mats Tech.

Kass, M. D., et al., 1998, Tribology Letters 5, pp. 231-234.

Kikuchi, K., et al., 2002, Proc. 5th Intl. Workshop on Spallation Mats. Tech.

Moraga, F., Taleyarkhan, R.P., 1999, Proc. Intl. Conf. on Accelerator Applications (AccApp'99), p. 301.

Pawel, S. J. and Mannes Schmidt, E. T., 2002, Proc. 5th Intl. Workshop on Spallation Mats. Tech.

Pointer W. D., et al., 2000, Proceedings of the ASME, FED-Vol. 253, p. 309.

Price, J. R., et al., 2003, Proc. 6th Intl. Conf. on Quality Control by Artificial Vision.

Riemer, B. W., et al., 1999, Proc. Intl. Conf. on Accelerator Applications (AccApp'99), p. 328.

Riemer, B.W., Hunn J. D., and Tsai, C.C., 2002, Proc. 5th Intl. Workshop on Spallation Mats. Tech.

Taleyarkhan, R.P. and F. Moraga, 2000, Nuclear Engineering and Design.

Wendel, M. W. and Haines, J. R., 2000, Proc. of the ASME Fluids Eng. Div. Summer Meeting, FEDSM2000-11005.

Wendel, M. W. and J. R. Haines, 2001, Proc. of ASME Fluids Eng. Div. Summer Meeting, FEDSM2001-18125.

Wendel, M. W., 2001, SNS Project Target Systems Report TSR-217.